



Enhancement of Visible Light Antibacterial Activities of Cellulose Fibers from Lotus Petiole Decorated ZnO Nanoparticles

Ngoc Hong Nguyen^{1,2} · Truong Phi Le^{2,3} · Trung Bao Ngoc Duong^{2,3} ·
Vien Ky Le^{2,3} · Hau Huu Do Ho^{1,2} · Linh Ho Thuy Nguyen^{2,4} · Tan Le Hoang Doan^{2,4} ·
Ngoc Xuan Dat Mai^{2,4} · Lan My Thi Nguyen^{2,3} · Ngoc Kim Pham^{1,2}

Accepted: 12 February 2024

© The Author(s), under exclusive licence to Springer Science+Business Media, LLC, part of Springer Nature 2024

Abstract

Cellulose/ZnO (CZ) nanocomposites are promising antimicrobial materials known for their antibiotic-free nature, biocompatibility, and environmental friendliness. In this study, cellulose fibers extracted from lotus petioles were utilized as a substrate and decorated with various shapes of ZnO nanoparticles (NPs), including small bean, hexagonal ingot-like, long cylindrical, and hexagonal cylinder-shaped NPs. Increasing zinc salt molar concentration resulted in highly crystalline ZnO NPs forming and enhanced interactions between ZnO NPs and -OH groups of cellulose. The thermal stability and UV–visible absorption properties of the CZ samples were influenced by ZnO concentration. Notably, at a ZnO molar ratio of 0.1, the CZ 0.1 sample demonstrated the lowest weight loss, while the optical band gap gradually decreased from 3.0 to 2.45 eV from the CZ 0.01 to CZ 1.0 samples. The CZ nanocomposites exhibited remarkable antibacterial activity against both *Staphylococcus aureus* (*S. aureus*, Gram-positive) and *Escherichia coli* (*E. coli*, Gram-negative) bacteria under visible light conditions, with a minimum inhibitory concentration (MIC) of 0.005 mg/mL for both bacterial strains. The bactericidal effects increased with higher concentrations of ZnO NPs, even achieving 100% inhibition. Incorporating ZnO NPs onto cellulose fibers derived from lotus plants presents a promising avenue for developing environmentally friendly materials with broad applications in antibacterial and environmental fields.

Keywords Zinc oxide · Cellulose fiber · Nanocomposites · Antibacterial · Lotus fiber

Ngoc Hong Nguyen and Truong Phi Le contributed equally to this work.

✉ Ngoc Kim Pham
phamkngoc@hcmus.edu.vn

¹ Faculty of Materials Science and Technology, University of Science, Ho Chi Minh City, Vietnam

² Vietnam National University, Ho Chi Minh City, Vietnam

³ Faculty of Biology and Biotechnology, University of Science, Ho Chi Minh City, Vietnam

⁴ Center for Innovative Materials and Architectures (INOMAR), Ho Chi Minh City, Vietnam

Introduction

In response to diminishing resources, pollution, and climate challenges, the bio-circular economy proposes a sustainable model transitioning from a carbon-intensive to a carbon-light economy [1]. Biochemical processes are initiated using renewable materials to produce biodegradable goods, stimulating the growth of sectors such as electronics, packaging, medical devices, and disposable products [2]. The emergence of scientific movements advocating for renewable resources and environmentally benign materials has generated considerable attention toward sustainable polymers, cellulose being a prominent illustration given its abundant presence in the natural world [3].

Cellulose, derived from many species, particularly plants, is a sustainable raw material supply that exhibits growth via photosynthesis [3–5]. Numerous studies have effectively isolated cellulose from agricultural waste and used it in many industrial applications [2]. The extensive use of this substance in many sectors, such as cosmetics, medicines, and food, may be attributed to its notable characteristics, which include non-toxicity and biocompatibility [6, 7]. Moreover, cellulose's distinctive structure allows alterations, expanding its range of uses.

The flexible nature of cellulose, attributed to its large surface area, mechanical qualities, and ability for modification, renders it a promising choice for a wide range of applications. These applications include several fields, such as water treatment, catalysis, and drug delivery systems [8]. Cellulose and its derivatives have shown exceptional performance as drug transporters and wound-healing agents within the medical domain, primarily owing to their remarkable biocompatibility [9].

Among the many sources of biomass materials, cellulose from lotus fiber, isolated from lotus petiole in Vietnam, can be justified by the following advantages. One of the most important is that lotus petiole is a bio-renewable and eco-friendly source of cellulose that has not been explored much before. Lotus petiole is rich in cellulose and has a unique helical coiled structure that can enhance the mechanical and thermal properties of the nanocomposites. The lotus fiber contains approximately $41.4 \pm 0.29\%$ cellulose and also exhibits high levels of hemicellulose, along with lignin (approximately $25.87 \pm 0.64\%$ and $19.56 \pm 0.32\%$, respectively) [10]. These components form a spiral twisted fiber structure organized in parallel along its length [11]. The diameter of lotus fibers ranges from 75 to 80 μm [12], and their length can extend from 10 to 20 cm while maintaining their shape [10, 11]. Due to the spiral twisted structure, lotus fibers possess excellent elasticity, enduring strong tensile forces without breaking. This outstanding property primarily arises from this unique structure, offering promising prospects for designing bio-materials with extraordinary mechanical characteristics [11].

Besides, lotus petiole is easy to collect and process; it falls off naturally from the plant and does not require harsh chemical treatments to isolate the cellulose. This reduces the environmental impact and the cost of production compared to conventional sources of cellulose, such as sugarcane bagasse, coconut husk fiber, and rice husk [13–15]. Nevertheless, the limits of its solubility and absence of antibacterial capabilities have prompted researchers to explore the development of improved nanocomposites by integrating nanoparticles [16].

Zinc oxide nanoparticles (ZnO NPs) are notable within metal nanoparticles due to their extensive uses and favorable safety characteristics [2]. Due to their dimensions and inherent characteristics, these entities possess the capacity to effectively initiate redox processes, making them an essential constituent in several domains [6, 17]. Numerous investigations

have examined techniques for fabricating zinc oxide nanostructures, aiming to achieve precise manipulation of their dimensions and morphology. Incorporating cellulose and ZnO in nanocomposites can augment antibacterial and photocatalytic functionalities [18–20]. This composite material provides an ecologically sustainable and biocompatible solution with exceptional mechanical qualities [21, 22]. Empirical evidence substantiates the compound's efficacy in combating bacterial strains, surpassing the performance of zinc oxide in isolation [2, 23]. The synthesis process encompasses chemical reactions in solutions containing alcohol or alkaline substances, offering a scalable and cost-effective alternative to physical methodologies.

The current study explores the potential of incorporating cellulose generated from lotus silk, a commonly accessible material, with safe metal salts to produce composites of CZ. The objective of this strategy is to improve the characteristics of cellulose by incorporating the antibacterial capabilities of ZnO, hence providing a cost-effective alternative to silver nanoparticles. The effectiveness of antimicrobial agents is contingent upon their concentration, therefore necessitating thorough examinations. The antibacterial processes of ZnO nanoparticles are comprehensively explained by practical observations and a detailed analysis of their activity.

Materials and Methods

Materials and Chemicals

Cellulose was isolated from lotus petiole and purified by chemical treatment, outlined briefly as follows. Lotus fibers (LF) were manually extracted from the petiole of lotus plants. The petiole was split, a center section was taken, and the outer skin was cut to reveal strands. These 2-cm-sliced strands were washed by ultrasonic treatment with various solvents, such as deionized water and an ethanol solution, to remove dust and impurities on their surface. Then, pre-cleansed fiber underwent bleaching with NaClO 8 wt% (7 h), hydrolysis with H₂SO₄ 60% (1 h), and finally immersion in a 1 M NaOH solution (2 h). All experimental processes are carried out at room temperature (30 °C). After that, the resulting cellulose fibers were purified and dried at 70 °C. Finally, the entire process aimed to obtain purified cellulose from lotus fibers.

Zinc acetate dihydrate (Zn(AC)₂·2H₂O) and NaOH were produced by Xilong Chemical Co., Ltd in China. Deionized (DI) water was utilized throughout all experimental procedures. All chemicals employed in this investigation were of analytical grade and used without additional purification.

Synthesis of Cellulose/ZnO Nanocomposites

Cellulose/ZnO nanocomposite materials were synthesized using chemical methods, as outlined in Fig. 1. A fixed amount of 0.02 g of cellulose was dispersed in 20 mL of deionized (DI) water at room temperature for 1 h. Simultaneously, solutions containing varying concentrations (0.01, 0.05, 0.1, 0.5, and 1 M) of dissolved Zn(AC)₂·2H₂O were prepared and subjected to magnetic stirring (details of ZnO molar concentration (M) and zinc acetate mass (g) are mentioned in Table 1). The zinc acetate solution was then combined with the cellulose matrix and heated at 90 °C for 1 h using a magnetic stirrer.

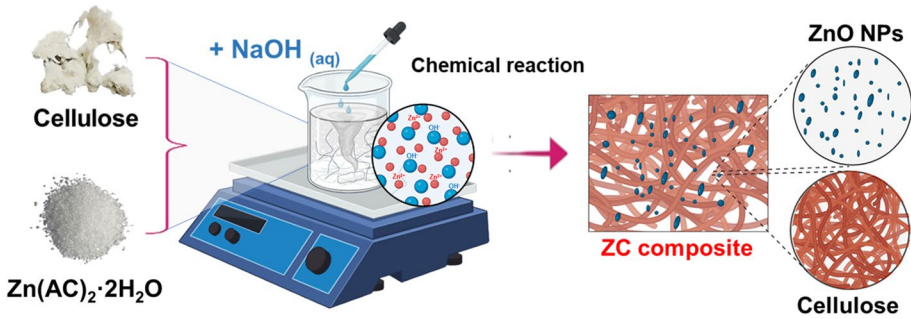


Fig. 1 Schematic diagram of CZ nanocomposites synthesis with ZnO nanoparticles

Table 1 The table summarizes the ZnO molar concentration value and zinc acetate mass (g) of each CZ sample

Sample	ZnO molar concentration (M)	Zinc acetate mass (g)
Cellulose	0	0
CZ 0.01	0.01	0.0439
CZ 0.05	0.05	0.2195
CZ 0.1	0.1	0.4389
CZ 0.5	0.5	2.1959
CZ 1	1	4.3898

As mentioned above, the synthesis of ZnO NPs involved the dropwise addition of 3 mL NaOH 1M solution into the mixture. The progress of the reaction was monitored based on the observed color change of the solution while maintaining a constant temperature of 90 °C and continuous magnetic stirring of 3 h. Subsequently, the resulting nanocomposites were centrifugated at 5000 rpm for 15 min and washed until the pH value approached 7. The CZ nanocomposites were then dried in an oven at 80 °C for 7 h. The resulting powder samples of the nanocomposites were denoted as CZ 0.01, CZ 0.05, CZ 0.1, CZ 0.5, and CZ 1, corresponding to the respective zinc nitrate concentrations of 0.01, 0.05, 0.1, 0.5, and 1 M, respectively.

The Properties of Cellulose/ZnO Nanocomposites

The structural characterization of the CZ nanocomposites was conducted using powder X-ray diffraction (p-XRD) with Cu K α radiation and a Ni filter ($\lambda = 1.5406$) at room temperature (RT). The measurements were performed on a D8 Advance Bruker system utilizing the Bragg–Brentano geometry. Fourier transform infrared analysis (FTIR) was carried out using a Bruker Tensor 27 to identify the chemical functional groups present in the sample. The surface morphology and particle shape were examined using scanning electron microscopy (SEM) with a Hitachi S4800 system, operating at an adjustable acceleration voltage of 10 kV. Thermal degradation behavior was studied using a TA Q500 Thermal Analysis system under a nitrogen atmosphere. The thermal stability of each sample was conducted at 25–700 °C with airflow at a rate of 10 °C/min. The optical properties of the

ZnO NPs were analyzed using ultraviolet–visible (UV–vis) spectroscopy with a Jasco 730 instrument. For UV–vis measurement, the synthesized CZ nanocomposites were dispersed uniformly in deionized (DI) water through sonication for 5 min to obtain a homogeneous solution.

Antimicrobial Testing Approach

Indicator Strains

Two different species of pathogenic bacteria, including *Escherichia coli* (ATCC 25922) and *Staphylococcus aureus* (ATCC BAA–1708), were provided by the Department of Plant Biotechnology and Biotransformation, University of Science, Ho Chi Minh City, Vietnam.

Determination of Minimum Inhibitory Concentrations (MICs) and Minimum Bactericidal Concentrations (MBCs)

Minimum inhibitory concentrations (MICs) are defined as the lowest concentration of an antimicrobial that will inhibit the visible growth of a microorganism after overnight incubation, and minimum bactericidal concentrations (MBCs) are defined as the lowest concentration of an antimicrobial agent that will prevent the development of an organism after subculture on to antibiotic-free media. MICs are often used as a research tool to determine MIC breakpoints [24].

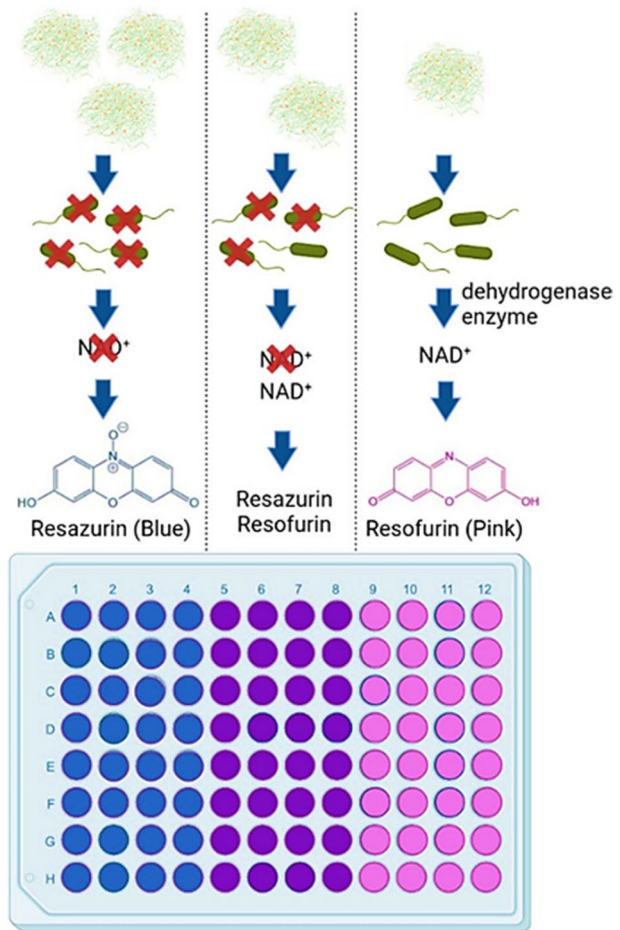
Resazurin MICs Procedure

MICs testing principle using resazurin (7-Hydroxy-3H-phenoxazin-3-one 10-oxide), an oxidation–reduction indicator, involves color changes to indicate bacterial viability or growth. Living bacterial cells maintain a reducing environment, containing dehydrogenase enzymes that reduce resazurin (blue and low fluorescent) to form resorufin (pink and high fluorescent) in Fig. 2. A pink color indicates a positive result, which also means that the bacteria remain viable in the presence of the material at the corresponding concentration. On the other hand, the blue color indicates a negative result, suggesting that the tested bacterial strains are inhibited or killed in the medium.

Antibacterial Test

The antibacterial efficacy of the CZ bio-nanocomposites against the bacteria *E. coli* (Gram-negative) and *S. aureus* (Gram-positive) was determined by using the Minimum Inhibitory Concentrations (MICs) and minimum bactericidal concentrations (MBCs) methods. The bacterial strains were cultured in Muller Hinton Broth (MHB) nutrient fluid and incubated on a shaker at 37 °C for 24 h in the standard atmosphere. The bacterial density was adjusted to 10^6 CFU/mL by measuring OD_{600nm} to ensure that a uniform number of bacteria was always used. A set of graphs of viability curves for each strain of bacterial species was prepared, resulting in highly active bacterial suspensions. The tested CZ samples were weighed and mixed in a 10% DMSO solution at concentrations of 0.075, 0.038, 0.019, 0.009, and 0.005 mg/mL.

Fig. 2 MICs and MBCs were tested for CZ products with different ZnO concentrations



The tested CZ eppendorfs were prepared consisting of 100 µl inoculum (10^6 CFU/mL), 800 µL Muller Hinton Broth (MHB), and 100 µL tested CZ samples, incubated at 37 °C for 24 h. Positive controls contain 100 µL of 3% streptomycin, replacing the tested CZ samples; negative controls do not add them. After 24 h, 40 µL of 0.01% resazurin reagent was added to each eppendorf, and the color change was observed after 15 min. The percentage of bacterial inhibition is determined using a specific formula Eq. (1):

$$\text{Bactericidal ratio (\%)} = \left(1 - \frac{T}{C}\right) \times 100 \tag{1}$$

C (control population) is viable cells at 24 h, and *T* (treatment population) is viable after the test. Subsequently, the tested CZ eppendorfs were evenly spread onto Muller Hinton Agar (MHA) plates and incubated at 37 °C for 24 h. Visible colonies were counted and reported as colony-forming units per milliliter (CFU/mL). The antibacterial activity was assessed by evaluating bacterial survival after exposure to the tested CZ and control samples. All experiments were conducted in triplicate, and data analysis, including standard deviation calculations and significance, was determined at a threshold of $p < 0.05$.

Results and Discussion

Microstructure of Cellulose/ZnO

The microstructures of cellulose and CZ nanocomposites influenced by the concentration of zinc salt precursors are illustrated in Fig. 3 through X-ray diffraction (XRD) and Fourier transforms infrared (FTIR) spectroscopy analyses. A sharp peak at 22° and broad peaks spanning the range of $16\text{--}18^\circ$ and 34.5° were assigned to cellulose (depicted by a black line), as shown in Fig. 3a. The peaks at 16° and 34° are identified as secondary peaks for the amorphous region of cellulose, while the primary peak at 22° signifies the crystalline cellulose region [25]. This correlation is associated with the crystalline phase of lotus silk, aligning with the crystal structure found in the literature by Di Liu and colleagues [26]. However, variations in peak intensity indicate alterations in cellulose crystallization in lotus fibers during acid hydrolysis. It can be said that the dissolution of the amorphous cellulose region in lotus fibers is evident during H_2SO_4 treatment, accompanied by the removal of low crystallinity non-cellulose components like pectin, lignin, and hemicellulose. This process contributes to an increased ratio of the crystalline region, indicating a restructuring of the crystal structure and an overall enhancement in cellulose crystallinity [12]. The details of the XRD and FTIR results of the cellulose extraction process from lotus silk are shown in Figure S1.

Each CZ pattern (Fig. 3a) revealed the presence of a consistent crystalline phase of ZnO in all CZ samples, with characteristic diffraction peaks observed at 2θ values of 31.7° , 34.5° , and 36.3° , corresponding to the (100), (002), and (101) lattice planes, respectively.

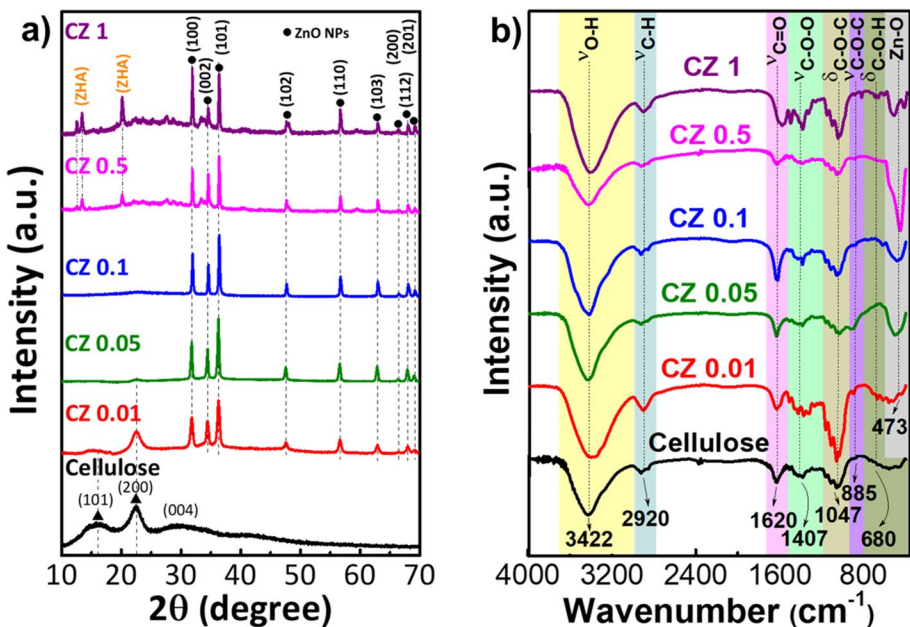
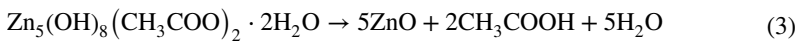
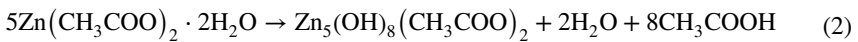


Fig. 3 **a** XRD and **b** FTIR spectra of CZ nanocomposites samples with different molar concentrations of ZnO NPs

Additionally, weak intensity peaks were observed at 2θ values of 47.7° , 56.7° , 62.8° , 66.4° , 67.9° , and 69.1° . These diffraction characteristics can be attributed to the hexagonal wurtzite structure and are consistent with the reference pattern of JCPDS:36–1451 [27]. The XRD peaks of the (101) and (200) lattice planes have poor intensity characteristics for cellulose material that appear in both samples (CZ 0.01 and 0.05).

In the case of the CZ 0.01 sample, which contains the lowest amount of ZnO, the primary diffraction peak of cellulose at the (200) plane shifts towards higher Bragg angles and demonstrates high intensity. Moreover, the diffraction peaks of cellulose in CZ 0.05 and CZ 0.1 are considerably weak compared to the prominent diffraction peak of ZnO, which indicates a high concentration of ZnO particles and their extensive growth on the cellulose surface within the CZ nanocomposites, making it challenging to obtain discernible diffraction data associated explicitly with cellulose. Another phase was identified in the CZ sample with the highest concentration of zinc salts (1 M and 0.5 M) at diffraction peaks with 2θ angles of 12.6° , 13.4° , and 20.1° , which were attributed to zinc hydroxide acetate (ZHA) [28]. ZHA is a byproduct of direct precipitation achieved by adding sodium hydroxide solution to an aqueous zinc acetate solution or stirring the ZnO powder with a zinc acetate solution. The presence of ZHA in the powder sample supports the proposed reaction mechanism, which is illustrated as follows [29]:



Hence, by analyzing the relative intensities of the peaks in samples CZ 1 and CZ 0.5, it can be concluded that zinc oxide is the predominant phase. However, they also exhibit a composite structure composed of zinc oxide, zinc acetate, and zinc hydroxide acetate integrated within the cellulose material. These findings indicate that the intercalation of ZnO nanoparticles (NPs) into the cellulose matrix does not alter the structural consistency but affects the molecular arrangement within the amorphous region of the cellulose matrix [8].

The FT-IR analysis results depicted in Fig. 3b illustrate the confirmation of the incorporation of concentration-differentiated ZnO nanoparticles (NPs) into the cellulose fiber structure, both before and after functionalization. The infrared spectra of the cellulose (black line) demonstrate distinct peaks for various functional groups. The broad peak at $3700\text{--}3000\text{ cm}^{-1}$ arises from stretching vibrations of the -OH group of absorbed H_2O and intramolecular OH group [30]. The stretching oscillations of -CH symmetric and asymmetric are reflected by the minimum at 2920 cm^{-1} . The characteristic vibrations of non-cellulose components, such as an absorption band at 1730 cm^{-1} corresponding to the stretching vibration of $\text{C}=\text{O}$ groups [25] aromatic ring stretching vibrations, do not appear in the FTIR spectrum of cellulose. The band at 1608 cm^{-1} is assigned to the bending vibrations of $\text{C}=\text{O}$ in the zinc acetate salt composition, and the bending oscillations of the in-plane OH bonds were determined at 1407 cm^{-1} and for 1047 cm^{-1} , a characteristic of the C-O stretched bond. The total CZ nanocomposites spectra all display the characteristic peaks of pristine cellulose, along with an additional peak at 473 cm^{-1} corresponding to ZnO NPs. It is easy to observe that the vibration of the Zn–O bond increases significantly with the addition of zinc acetate salt in the synthesis process [31]. However, at the highest zinc precursor content (CZ 1), the intensity of the ZnO peak decreases again. This change is revealed by the dominance of byproducts such as zinc hydroxide acetate (ZHA), as detailed in the discussion of XRD results [29].

Besides, the medium peak corresponding to C–O–O vibration in CZ samples is significantly less than that for the cellulose without ZnO NPs, confirming an oxidation process involving C-6, C–OH, and the glucose rings during the synthesis. Moreover, in the FTIR spectrum of the CZ nanocomposites, high-intensity bands at 1047 cm^{-1} and 3422 cm^{-1} exhibited a shift towards higher wave numbers, possibly indicating the interaction between ZnO nanoparticles (ZnO-NPs) and the OH group of cellulose fiber. The FTIR results complement the findings from XRD and SEM analyses.

Morphology and Elemental of Cellulose/ZnO Nanocomposites

The unmodified cellulose surface exhibits a smooth texture, with visible macro fibrils aligned along the fiber direction. The cellulose fiber prepared in this study demonstrated an average diameter of $1.74 \pm 0.51\ \mu\text{m}$ across all nanocomposite samples (Fig. 4a). Through the chemical precipitation method, ZnO nanostructures were successfully formed and adhered to the cellulose fiber, resulting in integration. CZ bio-nanocomposites show a dispersed arrangement of small-sized ZnO metal oxide clusters that can relatively identify the shape, size, and thickness of the cellulose fiber matrix. The concentration of Zn^{2+} influences the size distribution of ZnO NPs during synthesis. Figure 4b–f illustrate sparsely dispersed ZnO nanoparticles on the cellulose material. Sample CZ 0.01 exhibits small bean-shaped NPs with an average size of approximately 180 nm and random distribution. In sample CZ 0.05, the ZnO NPs grow with polymorphism and denser distribution. They gradually agglomerate into isolated large and small clusters due to the electrostatic attraction between Zn^{2+} and O^{2-} [31]. The nanoparticle size and dispersion variation exhibited significant differences as the concentration of ZnO in cellulose fiber increased. In the CZ 0.1 sample, the nanoparticles showed a more uniform and dense attachment to the cellulose matrix than in the CZ 0.5 and 1 samples. The CZ 0.1 nanoparticles displayed hexagonal ingot-like structures that fused, forming a $3.25\text{-}\mu\text{m}$ -thick outer shell of cellulose.

On the other hand, CZ 0.5 and 1 samples showed separate long cylindrical and hexagonal cylinder-shaped nanoparticles. Furthermore, increasing the quantity of ZnO-NPs on the

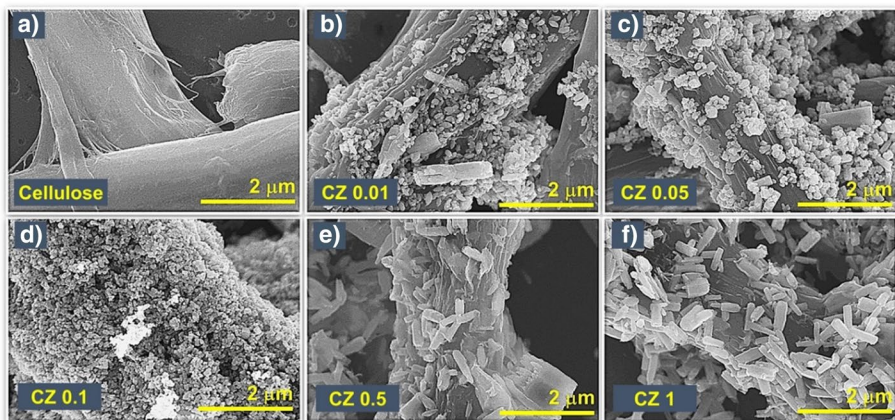


Fig. 4 SEM images of CZ nanocomposites samples: **a** cellulose, **b** 0.01, **c** 0.05, **d** 0.1, **e** 0.5, and **f** 1 M

cellulose surface enhanced the average particle diameter and length of ZnO-NPs. It should be noted that there was limited control over the size and morphology of the nanoparticles produced in all conducted experiments.

The constituents and distribution maps of the synthesized bionanomaterials were analyzed using EDX mapping spectroscopy (Fig. S1). The atoms were characterized by a monochromatic spot such as C (red) representing cellulose, Zn (blue) for ZnO, and O (green) being common to both. The successful intercalation of ZnO NPs on cellulose fiber was observed in both concentrations, as shown in Fig. S1(b, c). Zn atoms increased significantly from 6 to 38% and were densely distributed on the fiber surface. The increase in suspension due to zinc acetate salt content led to the severe aggregation of the $\text{Zn}(\text{OH})_3^-$, $\text{Zn}(\text{OH})_4^{2-}$, and ZnO NPs on the cellulose fiber surface, as discussed by SEM images. Based on this study, CZ 0.01 was the most suitable condition for embedding ZnO NPs on a cellulose matrix. Subsequently, the thermal properties of the CZ nanocomposites were investigated in detail using TGA analysis.

Thermal Properties of Cellulose/ZnO Nanocomposites

The thermal behavior of the bio-material was investigated by monitoring its weight changes as a function of temperature, as depicted in Fig. 5a. Thermogravimetric analysis (TGA) curves of the CZ samples, scanned from 25 to 700 °C, revealed a three-stage thermal degradation process [32]. Initially, the mass remained stable and approaching 100%. Subsequently, in the temperature range of 50–150 °C, the first stage of thermal decomposition occurred, resulting in a weight loss of 1–5%. This reduction can be attributed to the desorption of surface- or interstitial-bound water molecules and the release of low molecular weight organic compounds through oxidation and depletion processes in cellulosic polymers. The substantial second weight loss was observed in the temperature range of 250–400 °C, with CZ 0.01 exhibiting the highest loss at 58.67% in all cellulose functionalized with ZnO NPs. This significant weight reduction indicates the oxidative degradation of the cellulose, involving polymerization, dehydration, and glycosyl unit degradation, ultimately leading to residue formation. On the other hand, the thermal decomposition of $\text{Zn}(\text{OCOCH}_3)_2$ occurs upon heating at more than 147 °C and is very sensitive to the

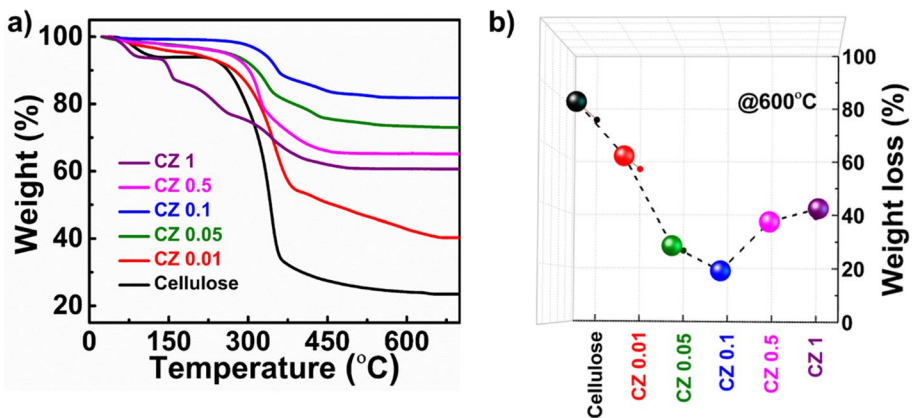
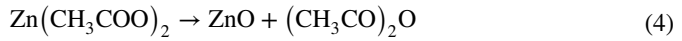


Fig. 5 a TGA curve from 10 °C to 700 °C and b weight loss at 600 °C of the difference molarity CZ samples

humidity of the surrounding air. As shown by reaction formula (3), the decomposition of zinc acetate and ZnO forming occurs through combustion or the release of acetic anhydride, as described overall below [28]:



The thermal decomposition behavior of CZ and cellulose differed; in detail, the CZ nanocomposite's weight degradation curves initiate at a higher maximum decomposition temperature than pristine cellulose (365 ° C). It indicates that nanocomposites CZ have superior thermal stability due to the catalytic activity of ZnO nanoparticles (NPs), which facilitated the accelerated decomposition of carbon cross-links within the cellulose matrix and also strong H-bonding interactions between ZnO and cellulose present in nanocomposites films alter their thermal properties [31]. The more salt precursors in synthesis, the higher the ZnO content embedded in the cellulose matrix, having fewer combustion residues. The loss weight percentages recorded at 600 ° C (Fig. 5b) were 75.86% (cellulose), 57.20% (CZ 0.01), 26.62% (CZ 0.05), 18.13% (CZ 0.1), 34.82% (CZ 0.5), and 39.31% (CZ 1), respectively. As pointed out, the heat endurance improvement performance of CZ material increases with high ZnO configuration and improves more than pristine cellulose [33]. Beyond 700 ° C, the total samples reached a thermal equilibrium state. Negligible mass losses of less than 1% were observed in this temperature range, indicating the release of trapped gases formed during the decomposition of acetate ions. In summary, heat-stable inorganic ZnO (as a solid-heat resistance incorporation of cellulose) enabled higher decomposition temperature and lower residual ash content.

Optical Properties

The optical properties of the cellulose and CZ samples, prepared at different ZnO concentrations, were investigated using UV–Vis absorption spectroscopy, as shown in Fig. 6a. The cellulose sample exhibited absorption peaks at 283 nm and 376 nm. Previous studies in the literature have proposed various explanations for the absorption peak at 283 nm in regenerated and acid-treated cellulose fiber, attributing it to the presence of carboxyl

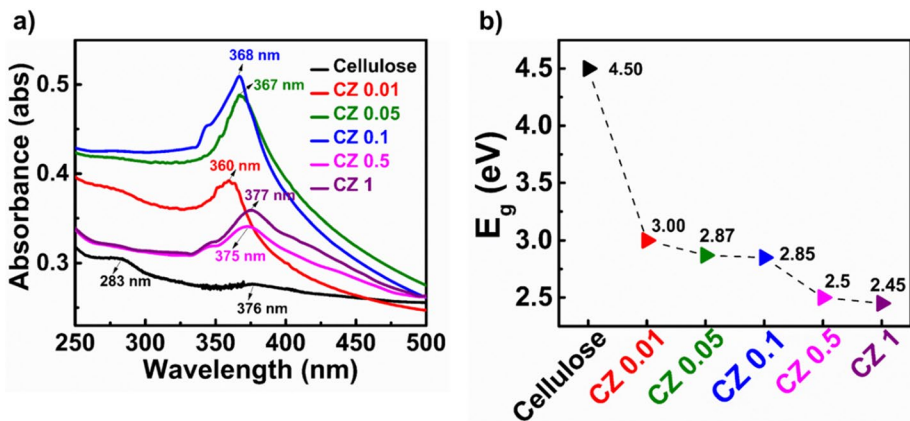


Fig. 6 UV–vis absorption spectra (a) of synthesized CZ with various molar concentrations and the corresponding E_g result (b)

groups generated during the treatment process. Additionally, the absorption peak at around 283 nm has been observed on the surface of cellulose treated with sulfate ions [34]. The cellulose polymer also exhibits a maximum absorbance at 304 nm [35]. The CZ displayed a distinct absorption peak at 360–377 nm, which can be attributed to ZnO's fundamental band gap absorption arising from the electronic transition from the valence to the conduction band ($O\ 2p \rightarrow Zn\ 3d$) [31]. This confirms the successful formation of ZnO nanoparticles on the surface of the cellulose fiber. Interestingly, a red shift in the absorption band was observed with increased ZnO size, indicating that larger ZnO nanoparticles can be obtained by increasing the concentration of Zn^{2+} ions. The band gap energy of the biological nano samples is according to the following Eq. (5):

$$\alpha h\nu = A(h\nu - E_g)^{n/2} \quad (5)$$

The determination of optical properties involves the analysis of critical parameters such as the band gap (E_g), light frequency (ν), and constant (A). In the case of ZnO, a direct transition is characterized by a value of n equal to 1. Utilizing this knowledge, we estimated the bandgap energies and ZnO particle sizes embedded within the cellulose fiber, as depicted in Fig. 6b. The findings demonstrate that the band gap of the hybrid material falls within the range of approximately 3.0 to 2.45 eV (Fig. S2), with increasing Zn^{2+} concentration. One plausible hypothesis for the reduction in bandgap as the concentration increment of ZnO is that the heightened concentration of ZnO results in an elevated amount of doping, introducing a more significant number of electrons into the conduction band [36]. This phenomenon results in a displacement of the Fermi level towards the edge of the conduction band, leading to a decrease in the effective bandgap [36]. These values exhibit a slight reduction compared to the reported band gap of pure ZnO films (3.23 eV), which can be ascribed to the heterostructure effect induced by the presence of cellulose during the mineralization process [3].

Antibacterial Activity of Cellulose/ZnO Nanocomposites

The antibacterial activity of the tested CZ nanocomposites mixture derived from lotus silk-based cellulose was evaluated against both *Staphylococcus aureus* (Gram-positive) and *Escherichia coli* bacteria (Gram-negative). These cellulose fibers incorporating ZnO particles exhibited an inhibition rate expressed as a percentage of bacterial reduction, as illustrated in Fig. 7. Bacterial quantification was performed using optical density measurements (OD_{600nm}) for both *S. aureus* and *E. coli* strains. The MIC results for both bacteria strains showed that the decoration of ZnO-NPs on the cellulose fiber effectively introduced antibacterial properties to the cellulose fiber (Fig. S4). In more detail, regarding the MIC values of CZ samples diluted from 5 to 75 ppm for the control sample, the reduction in *E. coli* populations was higher than that of *S. aureus* after 24 h under the same conditions. The broth dilution assay is an accurate and reliable method for determining the antibacterial activity of the examined nanoparticles.

The three samples with the highest ZnO concentration give information on the performance of activity antibacterials, which get 100% at five ppm for both viruses (Fig. 7 a and d), which can demonstrate that the higher the concentration of ZnO, the more influential the antibacterial activity. On the other hand, a minimal ZnO concentration of 0.01 M of the CZ mixture was used to demonstrate that it can suppress the development of *E. coli* and *S. aureus* between 38 and 75 ppm (Fig. 7 b and e). Likewise, the

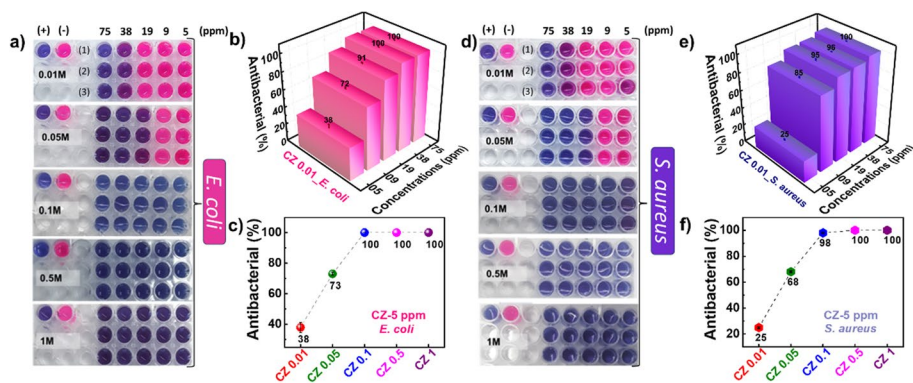


Fig. 7 MIC results for two bacterial strains, *E. coli* (a) and *S. aureus* (d), of all samples, bactericidal rate of 0.01 M CZ samples according to dilution concentrations (b, e) and the variation of bactericidal percentage according to 0.005 mg/mL content of CZ samples (c, f)

efficient CZ antibacterial agents are indicated by the measured MBC values of 38 ppm and 75 ppm for *E. coli* and *S. aureus*, respectively. Additionally, zinc oxide nanoparticles display successful antibacterial activities against various bacterial strains at even low concentrations, as demonstrated in work by Xie et al. [37]. The antibacterial effect of ZnO particles on Gram-negative and Gram-positive bacteria can be different because of the high susceptibility adjusted due to differences in the cell wall structure, exposure level, and different electrostatic affinities together.

A linear curve was plotted to comprehensively compare the antibacterial efficacy among all CZ samples, representing the percentage of antibacterial activity with a minimum sample concentration of 0.005 mg/mL (Fig. 7 c and f). It was observed that both bacterial strains tended to reach maximum bactericidal effects as the ZnO content in the samples increased, ultimately achieving 100% inhibition. These findings align with previous studies highlighting the antibacterial properties of bio-nanocomposites, wherein the presence of prerequisite inorganic nanoparticles, specifically ZnO, is supported and anchored by the underlying cellulose matrix. Moreover, numerous studies have validated the antibacterial activity of ZnO nanoparticles, and their underlying mechanisms of action have been extensively reported in the literature [8, 31, 38].

CZ nanocomposites have been investigated from various perspectives to elucidate their antibacterial mechanism, including the following aspects: (i) the ability to generate reactive oxidizing radicals (ROS), (ii) the release of Zn^{2+} , (iii) membrane dysfunction, and (iv) cell internalization. This work carried out an antibacterial activity under conditions without excitation light, and the size of ZnO particles was not tiny enough to diffuse through the membrane. Therefore, the release of Zn^{2+} and membrane dysfunction mechanism are proposed as the primary mechanism in this study. Typically, Zn^{2+} ions are released into the solution, which can be adsorbed onto the bacterial surface, facilitating their interaction with the cell membrane [39]. Another mechanism involves the physical properties of ZnO NPs and their electrostatic interaction with bacterial cells based on the principles of electrostatics. This electrostatic interaction promotes the adhesion of ZnO NPs to the cell surface, disrupting the electrical charge balance of the membrane and leading to structural distortions, morphological alterations, and, ultimately, cell death [40].

Conclusion

In conclusion, the investigation into CZ nanocomposites, specifically utilizing cellulose fibers from lotus plants adorned with various configurations of ZnO nanoparticles, has demonstrated their immense potential as antimicrobial materials. The synthesis process, influenced by the molar concentration of zinc salt, resulted in the formation of highly crystalline ZnO nanoparticles, fostering improved interactions with cellulose -OH groups. The CZ samples, particularly CZ 0.1, exhibited enhanced thermal stability and distinct UV–visible absorption characteristics. The optical band gap reduction observed with increasing ZnO concentration indicates the tunability of the CZ nanocomposites for specific applications. Remarkably, these materials exhibited outstanding antibacterial activity against Gram-positive *Staphylococcus aureus* and Gram-negative *Escherichia coli* under visible light conditions, with an MIC of 5 ppm for each bacterial strain. The bactericidal effects increased proportionally with the concentration of ZnO NPs, reaching a maximum of 100% inhibition. This research underscores the potential of incorporating ZnO NPs onto lotus plant-derived cellulose fibers, offering a promising avenue for developing eco-friendly materials.

Supplementary Information The online version contains supplementary material available at <https://doi.org/10.1007/s12010-024-04868-9>.

Acknowledgements The authors acknowledge the support of XRD, FTIR, and TGA measurements from the INOMAR Center, VNU-HCM.

Author Contribution N.H.N. and T.P.L.: methodology, investigation, writing-original draft. T.N.B.D.: data curation and investigation. V.K.L.: data curation. H.H.H.D.: methodology and writing-review. L.H.T.N. and T.L.H.D.: formal analysis. N.X.M.D.: validation. L.T.M.N.: conceptualization, writing-review and editing. N.K.P.: conceptualization, supervision, writing-review and editing.

Funding This research is funded by University of Science, VNU-HCM under grant number T2023-148.

Data Availability The data and materials are available from the corresponding author upon reasonable request.

Declarations

Ethical Approval Not applicable.

Consent to Participate Not applicable.

Consent for Publication Not applicable.

Competing Interests The authors declare no competing interests.

References

1. Wang, S., Yang, Y., Lu, A., & Zhang, L. (2019). Construction of cellulose/ZnO composite microspheres in NaOH/zinc nitrate aqueous solution via one-step method. *Cellulose*, 26(1), 557–568. <https://doi.org/10.1007/s10570-018-2201-9>
2. Elemike, E. E., Onwudiwe, D. C., & Mbonu, J. I. (2021). Facile synthesis of cellulose–ZnO-hybrid nanocomposite using *Hibiscus rosa-sinensis* leaf extract and their antibacterial activities. *Applied Nanoscience (Switzerland)*, 11(4), 1349–1358. <https://doi.org/10.1007/s13204-021-01774-y>

3. Fu, F., Gu, J., Xu, X., Xiong, Q., Zhang, Y., Liu, X., & Zhou, J. (2017). Interfacial assembly of ZnO–cellulose nanocomposite films via a solution process: A one-step biomimetic approach and excellent photocatalytic properties. *Cellulose*, 24(1), 147–162. <https://doi.org/10.1007/s10570-016-1087-7>
4. Lefatshe, K., Muiva, C. M., & Kebaabetswe, L. P. (2017). Extraction of nanocellulose and in-situ casting of ZnO/cellulose nanocomposite with enhanced photocatalytic and antibacterial activity. *Carbohydrate Polymers*, 164, 301–308. <https://doi.org/10.1016/j.carbpol.2017.02.020>
5. Ibahim, N. A., Eid, B. M., El-Aziz, E. A., & Abou Elmaaty, T. M. (2013). Functionalization of linen/cotton pigment prints using inorganic nano structure materials. *Carbohydrate Polymers*, 97(2), 537–545. <https://doi.org/10.1016/j.carbpol.2013.04.084>
6. Ul-Islam, M., Khattak, W. A., Ullah, M. W., Khan, S., & Park, J. K. (2014). Synthesis of regenerated bacterial cellulose-zinc oxide nanocomposite films for biomedical applications. *Cellulose*, 21(1), 433–447. <https://doi.org/10.1007/s10570-013-0109-y>
7. Zheng, J., Choo, K., Bradt, C., Lehoux, R., & Rehmann, L. (2014). Enzymatic hydrolysis of steam exploded corn cob residues after pretreatment in a twin-screw extruder. *Biotechnology Reports*, 3, 99–107. <https://doi.org/10.1016/j.btre.2014.06.008>
8. Dawwam, G. E., Al-Shemy, M. T., & El-Demerdash, A. S. (2022). Green synthesis of cellulose nanocrystal/ZnO bio-nanocomposites exerting antibacterial activity and downregulating virulence toxigenic genes of food-poisoning bacteria. *Scientific Reports*, 12(1). <https://doi.org/10.1038/s41598-022-21087-6>
9. Seddiqi, H., Oliaei, E., Honarkar, H., Jin, J., Geonzon, L. C., Bacabac, R. G., & Klein-Nulend, J. (2021, March 1). Cellulose and its derivatives: towards biomedical applications. *Cellulose*. Springer Science and Business Media B.V. <https://doi.org/10.1007/s10570-020-03674-w>
10. Pan, Y., Han, G., Mao, Z., Zhang, Y., Duan, H., Huang, J., & Qu, L. (2011). Structural characteristics and physical properties of lotus fibers obtained from *Nelumbo nucifera* petioles. *Carbohydrate Polymers*, 85(1), 188–195. <https://doi.org/10.1016/j.carbpol.2011.02.013>
11. Guan, Q. F., Han, Z. M., Zhu, Y., Xu, W. L., Yang, H. Bin, Ling, Z. C., ... Yu, S. H. (2021). Bio-inspired lotus-fiber-like spiral hydrogel bacterial cellulose fibers. *Nano Letters*, 21(2), 952–958. <https://doi.org/10.1021/acs.nanolett.0c03707>
12. Cheng, C., Guo, R., Lan, J., & Jiang, S. (2017). Extraction of lotus fibres from lotus stems under microwave irradiation. *Royal Society Open Science*, 4(9). <https://doi.org/10.1098/rsos.170747>
13. Sharma, J. L., Sharma, R. K., Kumari, M., Choudhary, B. L., & Dhayal, V. (2021). Modification of cellulose with ZnO nanoparticles: From sugarcane bagasse to antimicrobial composite. *Journal of Nano and Electronic Physics*, 13(5), 1–5. [https://doi.org/10.21272/JNEP.13\(5\).05028](https://doi.org/10.21272/JNEP.13(5).05028)
14. Wasim, M., Shi, F., Liu, J., Farooq, A., Khan, S. U., Salam, A., ... Zhao, X. (2021, September 1). An overview of Zn/ZnO modified cellulosic nanocomposites and their potential applications. *Journal of Polymer Research*. Springer Science and Business Media B.V. <https://doi.org/10.1007/s10965-021-02689-6>
15. Nang An, V., Chi Nhan, H. T., Tap, T. D., Van, T. T. T., Van Viet, P., & Van Hieu, L. (2020). Extraction of high crystalline nanocellulose from biorenewable sources of Vietnamese agricultural wastes. *Journal of Polymers and the Environment*, 28(5), 1465–1474. <https://doi.org/10.1007/s10924-020-01695-x>
16. Sulaeva, I., Henniges, U., Rosenau, T., & Potthast, A. (2015). Bacterial cellulose as a material for wound treatment: Properties and modifications: A review. *Biotechnology Advances*. Elsevier Inc. <https://doi.org/10.1016/j.biotechadv.2015.07.009>
17. Grönqvist, S., Kampuri, T., Maloney, T., Vehviläinen, M., Liitiä, T., & Suurnäkki, A. (2015). Enhanced pre-treatment of cellulose pulp prior to dissolution into NaOH/ZnO. *Cellulose*, 22(6), 3981–3990. <https://doi.org/10.1007/s10570-015-0742-8>
18. Cheng, F., Betts, J. W., Kelly, S. M., Wareham, D. W., Kornherr, A., Dumestre, F., ... Heinze, T. (2014). Whiter, brighter, and more stable cellulose paper coated with antibacterial carboxymethyl starch stabilized ZnO nanoparticles. *Journal of Materials Chemistry B*, 2(20), 3057–3064. <https://doi.org/10.1039/c3tb21734e>
19. Jiao, L., Ma, J., & Dai, H. (2015). Preparation and characterization of self-reinforced antibacterial and oil-resistant paper using a NaOH/Urea/ZnO solution. *Plos One*, 10(10), 1–16. <https://doi.org/10.1371/journal.pone.0140603>
20. Azizi, S., Ahmad, M. B., Ibrahim, N. A., Hussein, M. Z., & Namvar, F. (2014). Cellulose nanocrystals/ZnO as a bifunctional reinforcing nanocomposite for poly(vinyl alcohol)/chitosan blend films: Fabrication, characterization and properties. *International Journal of Molecular Sciences*, 15(6), 11040–11053. <https://doi.org/10.3390/ijms150611040>
21. Chauhan, I., Aggrawal, S., & Mohanty, P. (2015). ZnO nanowire-immobilized paper matrices for visible light-induced antibacterial activity against *Escherichia coli*. *Environmental Science: Nano*, 2(3), 273–279. <https://doi.org/10.1039/c5en00006h>
22. Espitia, P. J. P., Soares, N. D. F. F., Coimbra, J. S. D. R., de Andrade, N. J., Cruz, R. S., & Medeiros, E. A. A. (2012). Zinc oxide nanoparticles: Synthesis, antimicrobial activity and food

- packaging applications. *Food and Bioprocess Technology*, 5(5), 1447–1464. <https://doi.org/10.1007/s11947-012-0797-6>
23. Zare-Akbari, Z., Farhadnejad, H., Furughi-Nia, B., Abedin, S., Yadollahi, M., & Khorsand-Ghayeni, M. (2016). PH-sensitive bionanocomposite hydrogel beads based on carboxymethyl cellulose/ZnO nanoparticle as drug carrier. *International Journal of Biological Macromolecules*, 93, 1317–1327. <https://doi.org/10.1016/j.ijbiomac.2016.09.110>
 24. Andrews, J. M. (2001). Determination of minimum inhibitory concentrations. *Journal of Antimicrobial Chemotherapy*, 48(suppl_1), 5–16. https://doi.org/10.1093/jac/48.suppl_1.5
 25. Cheng, C., Guo, R., Lan, J., Jiang, S., Du, Z., Zhao, L., & Peng, L. (2018). Preparation and characterization of lotus fibers from lotus stems. *Journal of the Textile Institute*, 109(10), 1322–1328. <https://doi.org/10.1080/00405000.2018.1423898>
 26. Liu, D., Han, G., Huang, J., & Zhang, Y. (2009). Composition and structure study of natural *Nelumbo nucifera* fiber. *Carbohydrate polymers*, 75(1), 39–43.
 27. Khorsand Zak, A., Abd. Majid, W. H., Abrishami, M. E., & Yousefi, R. (2011). X-ray analysis of ZnO nanoparticles by Williamson-Hall and size-strain plot methods. *Solid State Sciences*, 13(1), 251–256. <https://doi.org/10.1016/j.solidstatesciences.2010.11.024>
 28. Aoji, H., & Shiomi, H. (2020). Effects of aging conditions on the morphologies of ZnO particles synthesized under hydrothermal conditions from layered zinc hydroxide as a precursor derived from zinc acetate. *Journal of Asian Ceramic Societies*, 8(1), 81–93. <https://doi.org/10.1080/21870764.2019.1709692>
 29. Luković Golić, D., Branković, G., Počuča Nešić, M., Vojisavljević, K., Rečnik, A., Daneu, N., ... Branković, Z. (2011). Structural characterization of self-assembled ZnO nanoparticles obtained by the sol-gel method from Zn(CH₃COO)₂·2H₂O. *Nanotechnology*, 22(39). <https://doi.org/10.1088/0957-4484/22/39/395603>
 30. Hasanpour, M., Motahari, S., Jing, D., & Hatami, M. (2021). Investigation of the different morphologies of zinc oxide (ZnO) in cellulose/ZnO hybrid aerogel on the photocatalytic degradation efficiency of methyl orange. *Topics in Catalysis*, (0123456789). <https://doi.org/10.1007/s11244-021-01476-3>
 31. Wahid, F., Duan, Y., Hu, X., Chu, L., Jia, S., Cui, J., & Zhong, C. (2019). International Journal of Biological Macromolecules A facile construction of bacterial cellulose/ZnO nanocomposite films and their photocatalytic and antibacterial properties. *International Journal of Biological Macromolecules*, 132, 692–700. <https://doi.org/10.1016/j.ijbiomac.2019.03.240>
 32. Li, X., Li, H., Wang, X., Xu, D., You, T., Wu, Y., & Xu, F. (2021). International Journal of Biological Macromolecules Facile in situ fabrication of ZnO-embedded cellulose nanocomposite films with antibacterial properties and enhanced mechanical strength via hydrogen bonding interactions. *International Journal of Biological Macromolecules*, 183, 760–771. <https://doi.org/10.1016/j.ijbiomac.2021.04.175>
 33. Onyszko, M., Szczupak, A. M., Rakoczy, R., Paszkiewicz, O., & Janusz, J. (2022). The cellulose fibers functionalized with star-like zinc oxide nanoparticles with boosted antibacterial performance for hygienic products. *Scientific Reports*, 1–13. <https://doi.org/10.1038/s41598-022-05458-7>
 34. Yu, H. Y., Chen, G. Y., Wang, Y. B., & Yao, J. M. (2015). A facile one-pot route for preparing cellulose nanocrystal/zinc oxide nanohybrids with high antibacterial and photocatalytic activity. *Cellulose*, 22(1), 261–273. <https://doi.org/10.1007/s10570-014-0491-0>
 35. Arza, C. R., Ilk, S., Demircan, D., & Zhang, B. (2018). New biobased non-ionic hyperbranched polymers as environmentally friendly antibacterial additives for biopolymers. *Green Chemistry*, 20(6), 1238–1249. <https://doi.org/10.1039/c7gc03401f>
 36. Lu, J. G., Fujita, S., Kawaharamura, T., Nishinaka, H., Kamada, Y., Ohshima, T., ... Zhao, B. H. (2007). Carrier concentration dependence of band gap shift in n-type ZnO:Al films. In *Journal of Applied Physics* (Vol. 101). <https://doi.org/10.1063/1.2721374>
 37. Xie, Y., He, Y., Irwin, P. L., Jin, T., & Shi, X. (2011). Antibacterial activity and mechanism of action of zinc oxide nanoparticles against *Campylobacter jejuni*. *Applied and Environmental Microbiology*, 77(7), 2325–2331. <https://doi.org/10.1128/AEM.02149-10>
 38. Zhao, S.-W., Guo, C.-R., Hu, Y.-Z., Guo, Y.-R., & Pan, Q.-J. (2018). The preparation and antibacterial activity of cellulose/ZnO composite: A review. *Open Chemistry*, 16(1), 9–20. <https://doi.org/10.1515/chem-2018-0006>
 39. Pasquet, J., Chevalier, Y., Pelletier, J., Couval, E., Bouvier, D., & Bolzinger, M.-A. (2014). The contribution of zinc ions to the antimicrobial activity of zinc oxide. *Colloids and Surfaces A: Physicochemical and Engineering Aspects*, 457, 263–274. <https://doi.org/10.1016/j.colsurfa.2014.05.057>

40. Sirelkhatim, A., Mahmud, S., & Seeni, A. (2015). Review on zinc oxide nanoparticles: Antibacterial activity and toxicity mechanism. *Nano-Micro Letters*. <https://doi.org/10.1007/s40820-015-0040-x>

Publisher's Note Springer Nature remains neutral with regard to jurisdictional claims in published maps and institutional affiliations.

Springer Nature or its licensor (e.g. a society or other partner) holds exclusive rights to this article under a publishing agreement with the author(s) or other rightsholder(s); author self-archiving of the accepted manuscript version of this article is solely governed by the terms of such publishing agreement and applicable law.